IEEE Access
Multidisciplinary | Rapid Review | Open Access Journal

Received June 12, 2019, accepted July 2, 2019, date of publication July 8, 2019, date of current version July 25, 2019.

Digital Object Identifier 10.1109/ACCESS.2019.2927280

The Circular Polarization Diversity Antennas Achieved by a Fractal Defected Ground Structure

KUN WEI[1], BOCHENG ZHU[1], AND MINGLIANG TAO[2]
[1]Department of Electronics, School of Electronics Engineering and Computer Science, Peking University, Beijing 100871, China
[2]School of Electronics and Information, Northwestern Polytechnical University, Xi'an 710072, China

Corresponding author: Kun Wei (weikun916@163.com)

This work was supported in part by the Postdoctoral Innovative Talent Support Program under Grant BX20180003, in part by the State Administration of Science, Technology and Industry for National Defense under Grant JCKY2016110B004, and in part by the China Postdoctoral Science Foundation under Grant 2018M631258.

ABSTRACT This paper proposes the circularly polarized (CP) antennas with a restored radiation pattern for the polarization diversity applications. The proposed CP antennas have dual polarizations, the left-handed circularly polarized (LHCP) antenna is designed for transmitting and the right-handed circularly polarized (RHCP) antenna is designed for receiving. The CP antenna operation and the radiation pattern restoration are realized by a fractal defected ground structure (FDGS). When achieving the radiation pattern restoration, the proposed CP antennas forward efficiencies are improved from 66.8% to 81% and the forward realized gains are improved from 2.56 dBi to 5.38 dBic, respectively.

INDEX TERMS Radiation pattern restoration, defected ground structure, fractal structure, circular polarization, polarization diversity.

I. INTRODUCTION

Diversity proved to be an effective solution to mitigate multipath fading signals and enhance the system capacity. The most popular diversity technique is the antenna diversity which can be classified as spatial/space, polarization and pattern diversities [1]–[4]. The CP microstrip antenna is popularly studied because it reduces the signal polarization misalignment [5]. When the circular polarization diversity antennas are closely placed, the antenna settlement will cause antenna radiation pattern deviation, forward gain and efficiency degradation. Therefore, the CP antennas with the radiation pattern restoration play an important role in the polarization diversity applications [6].

Some polarization diversity antennas achieved by the cross-shaped dipoles or dielectric resonator antennas have been studied. A polarization diversity antenna is presented in [7]. The folded dipole antenna with a protruding part is used as a $+45$ polarization element and another folded dipole with a concave part is used as a -45 polarization element. A multifunction cross-shaped dielectric resonator antenna with separately fed CP and linearly polarized (LP) radiation patterns is proposed in [8]. The proposed antenna could be used as polarization diversity antenna due to the overlapping dual-feed CP and LP operation. The design for antenna with the polarization diversity is described in [9]. The antenna structure is mainly composed of a reconfigurable crossed-dipole fed with a coaxial baluns and a switchable feeding network. By controlling the states of pin diodes embedded in the balun feeds, the integrated antenna can offer four polarization modes, including $\pm 45°$ LPs, RHCP and LHCP. A dual-LP antenna and an integrated dual-CP antenna are proposed in [10]. The feeding networks and the radiators are printed on two sides of a substrate, forming a fully planar structure. In order to achieve $\pm 45°$ polarizations or CP polarization, two dipoles are fed by two balun-included feeding networks. These polarization diversity antennas need complex feeding network to excite the antenna elements for achieving the CP operation, which increases the antenna profile.

The CP microstrip antennas for the polarization diversity application have been reported. The study of a 2×2 circular disc array antenna with polarization diversity is studied in [11]. Each disc element is located above a circular slot fed by an L-shaped strip, in which the switching between two orthogonal LP and CP are realized by controlling two pin diodes. A mechanically reconfigurable patch antenna with polarization diversity is presented in [12]. The antenna is composed of a fixed L-probe feed on a bottom substrate layer

The associate editor coordinating the review of this manuscript and approving it for publication was Kai Lu.

and a patch with truncated corners on an upper substrate layer that can rotate in azimuth. The handedness of the circular polarization (RHCP or LHCP) may be changed by simply rotating the upper substrate by 90° with respect to the fixed capacitively coupled feed. Those research works need multi-layer and special feeding structure to achieve the CP radiation and polarization diversity, which increases the antenna structure complexity.

Some cross-placed printed antennas for the polarization diversity application have also been studied. A planar antenna pair has been developed to achieve the polarization diversity is proposed in [13]. The technique is developed to force one printed patch to play two roles and hence to achieve polarization diversity using only three printed patches, as opposed to four in a conventional diversity pair. A uniplanar polarization diversity differential antenna is presented in [14]. The antenna employs octagonal-shaped slot and two pairs of differentially fed monopoles being orthogonal to each other to achieve the polarization diversity performance. A uniplanar polarization diversity antenna with dual band-notched characteristics is presented in [15]. The antenna employs orthogonal feeding structure to achieve polarization diversity performance. A new compact coplanar-fed antenna suitable for polarization diversity application is presented in [16]. The antenna consists of two identical monopoles that are printed on a low-loss substrate and positioned perpendicular to each other. Those related research works also need feeding network to achieve CP operation and do not take the antenna radiation pattern restoration into consideration.

By adding the parasitic strip, the antennas CP operation and the radiation pattern restoration are realized in [17]. However, the antennas are not designed for the polarization diversity application. This paper proposes the CP antennas with the radiation pattern restoration for the polarization diversity system. The proposed CP antennas have dual polarizations, the left placed antenna resonates in the LHCP mode for transmitting and the right placed antenna resonates in the RHCP mode for receiving. The FDGS is applied to design the CP operation and to achieve the radiation patterns restoration. The restored radiation patterns will contribute to increase the antenna forward realized gain and efficiency. Table 1 lists the comparisons of this work and previous published circular polarization diversity antennas. It shows the proposed circular polarization diversity antennas achieved by the FDGS in this paper has a simple structure and the radiation pattern restoration.

This paper is organized as follows. Section II shows the geometries of the designed FDGS and the CP antennas, as well as the parameter study. Section III illustrates the antenna forward gain and efficiency improvements. Section IV indicates the simulated and measured results comparisons. While section V gives the conclusions.

II. ANTENNA GEOMETRY AND PARAMETER STUDY

Fig. 1 shows the CP antennas and the FDGS geometries. The CP antennas, resonant at the GPS-L1 band, are collinearly

TABLE 1. Comparisons of polarization diversity antennas.

Ref.	Antenna type	CP achieved method	Radiation pattern restoration
[9]	crossed-dipoles	feeding network	No
[10]	crossed-dipoles	feeding network	No
[12]	Microstrip antenna	L-shaped feeding structure	No
[13]	cross-placed printed antennas	feeding network	No
[15]	cross-placed printed antennas	feeding network	No
[17]	Microstrip antennas	parasitic strip	YES
This work	Microstrip antennas	Fractal DGS	YES

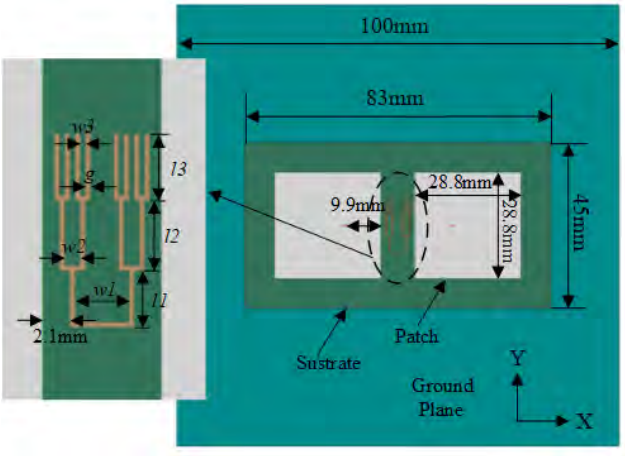

FIGURE 1. Geometries of the proposed FDGS structure and the CP microstrip antennas.

settled on the x axis. The left and the right placed antennas work in the LHCP mode and the RHCP mode, respectively. The antenna patches are printed on a substrate Taconic CER-10, which has the dimension 83 × 45 mm^2, thickness 3.18 mm and the dielectric constant 10. The edge-to-edge and center-to-center distances between the antenna patches are 9.2 mm (0.048 λ_0) and 38 mm (0.2 λ_0), respectively. The proposed U-shaped FDGS for realizing the CP antennas design and the radiation pattern restoration is also drawn in Fig. 1. The designed U-shaped FDGS is etched away from the ground plane with the dimension 100 × 100 mm^2.

The proposed fractal structure, as shown in Fig. 2, is evolved from the classic U-shaped structure. Adding two diminutive U-shaped slots at the endpoints of a basic U-shaped slot turns the zero iterative fractal structure into the first iterative fractal structure, as drawn in Fig. 2 (b). The third iterative fractal structure is evolved from the second iterative fractal structure by adding four U-shaped slots at the endpoints. By repeating this process, the high level iterative fractal structures are designed.

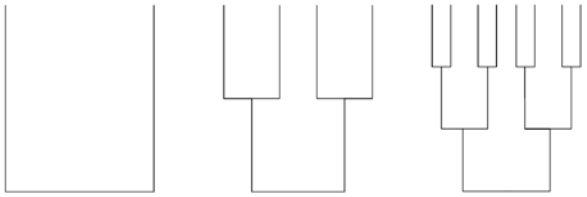

FIGURE 2. The proposed fractal DGS (a) zero iteration (b) first iteration (c) second iteration.

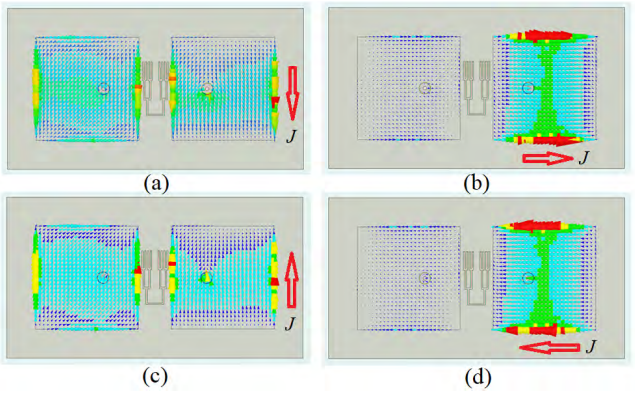

FIGURE 3. Current vectors distributions on the patches at different time phases (a) 0°, (b) 90°, (c) 180°, (d) 270°.

For understanding how the antenna CP operation is achieved by the proposed FDGS, the current distributions on the patches are studied. The surface currents vectors of the antenna patches with the proposed FDGS are shown in Fig. 3, when only exciting the right positioned antenna. These four subgraphs show the surface current vectors at different time phases (ωt), from 0° to 270° with an interval of 90°. As shown in the subgraph (b) and subgraph (d), the horizontal surface current distributions are detected only on the right placed antenna, which contributes to generate the electric field E_x on the x axis. Before the FDGS is etched in the ground plane, there is barely vertical surface current distribution on the patches. As shown in the subgraph (a) and subgraph (c), the vertical current distributions are detected on both the patches because of the FDGS in the ground plane. The vertical surface current distributions on both the patches contribute to generate the electric field E_y on the y axis. When the electric field E_x and E_y have the same magnitude, the right placed antenna achieves the CP operation. Moreover, the surface current vectors are anticlockwise, which means the right placed antenna works in the RHCP mode. When only exciting the left positioned antenna, the same principle for achieving the CP operation will be got. The difference is that the left positioned antenna works in the LHCP mode.

Comparing to the antennas without the FDGS, the patches have current vectors in the vertical direction when etching the FDGS in the ground plane, as shown in Fig. 3. These current vectors in the vertical direction, as well as the current vectors in the horizontal direction contribute to achieve

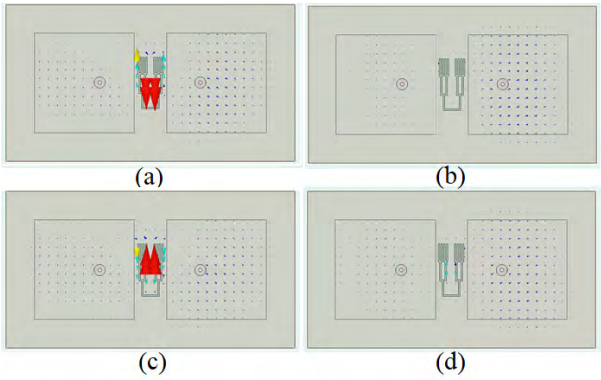

FIGURE 4. Current vectors distributions on the ground plane at different time phases (a) 0°, (b) 90°, (c) 180°, (d) 270°.

the CP operation. In order to explain why both the patches have the current vectors in the vertical direction, the current distribution in the ground plane with the FDGS is studied. Fig. 4 shows the surface current vectors in the ground plane with the proposed FDGS, when only exciting the right positioned antenna. These four subgraphs show the surface current vectors at different time phases (ωt), from 0° to 270° with an interval of 90°. At time phase 0°, the FDGS is coupled fed to have the current vectors in the vertical direction, as shown in Fig. 4 (a). With the help of this current distribution, both the patches are coupled to have the current vectors in the vertical direction, as shown in Fig. 3 (a). The proposed FDGS is coupled by the excited patch and has the current vectors in the vertical direction. The other way around, both the patches are coupled by the FDGS to have the current vectors in the vertical direction. Because of the FDGS in the ground plane, the patches have the current vectors in the vertical direction. The antenna CP operation is achieved because the existence of the current vectors in the vertical direction, as well as the current vectors in the horizontal direction.

By the parameters sweep and optimization, the antennas and the FDGS optimized parameters values are: $w1 = 4.2$ mm, $w2 = 1.2$ mm, $w3 = 0.4$ mm, $l1 = 4.4$ mm, $l2 = 5.4$ mm, $l3 = 5.2$ mm and $g = 0.4$ mm. The simulation studies carried out by the Ansoft High Frequency Structure Simulator (HFSS) are applied to investigate the antennas performances. The FDGS width and length affect the antenna performance most. Which means the FDGS dimension optimization will help to achieve the better antenna CP performance.

Fig. 5 (a) gives the S11 (return loss) of the right placed CP antenna, when tuning the FDGS length $l3$ from 4.8 mm to 5.6 mm. It clearly shows that the antennas with the FDGS have two resonant modes. Since the electric field E_x on the x axis is generated by the horizontal surface current distributions on the right placed antenna, this resonant mode is fixed in the low frequency region. Another resonant mode is determined by the electric field E_y on the y axis, which is generated by the vertical surface current distributions on both patches. The resonant mode on the y axis shifts to low

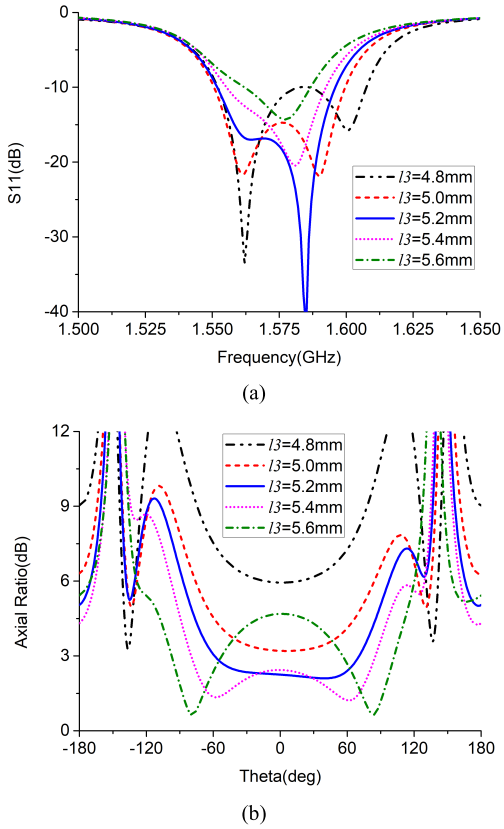

FIGURE 5. The (a) S11 and (b) the AR of the right placed CP antenna when tuning the FDGS length *l3*.

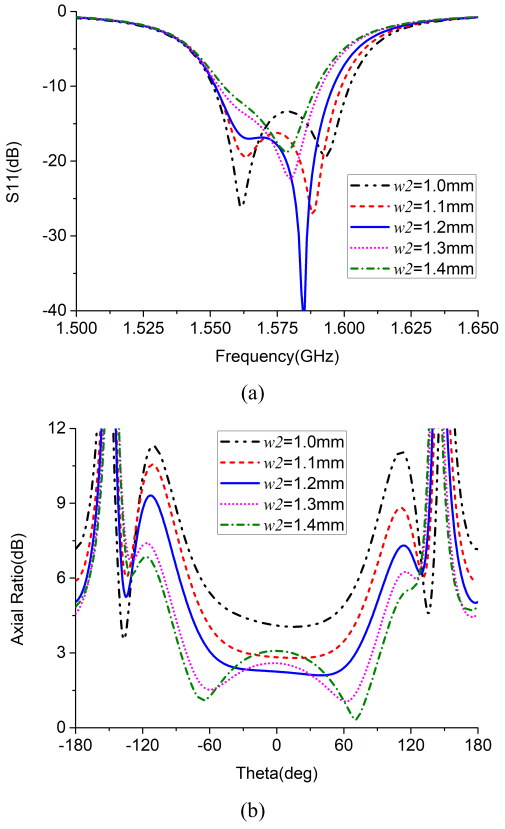

FIGURE 6. The (a) S11 and (b) the AR of the right placed CP antenna when tuning the FDGS width *w3*.

frequency region when increasing the FDGS length *l3*. When tuning the FDGS length *l1* and *l2*, the same conclusion can be got. By optimizing the FDGS length, those two orthogonal resonant modes should have the 90° time-phase difference and the same magnitude. Because of that, the right placed antenna achieves CP operation. Fig. 5 (b) gives the right placed antenna axial ratio (AR) against theta, when turning the FDGS length *l3* from 4.4 mm to 5.2 mm. It shows when the FDGS length *l3* is close to 5.2 mm, the antennas have the better CP performances.

Fig. 6 (a) illustrates the right placed antenna S11 against frequency, when tuning the FDGS width *w2* from 0.8 mm to 1.5 mm. There are two resonant modes occur after the proposed FDGS etched away from the ground plane. The lower frequency resonant mode is generated by the electric field E_x on the x axis. This resonant mode is fixed at certain frequency, because the patch physical dimensions are not changed. The second orthogonal resonant mode is determined by the electric field E_y on the y axis. When increasing the FDGS width *w2*, the second orthogonal resonant mode moves to lower frequency region. After optimizing the FDGS dimension, the right placed antenna will achieve the CP operation when those two orthogonal modes have the same magnitude and 90° time-phase difference. The antenna ARs against the FDGS width *w2* are shown in Fig. 6 (b). When the FDGS width *w2* is closer to 1.2 mm, the antenna CP performance

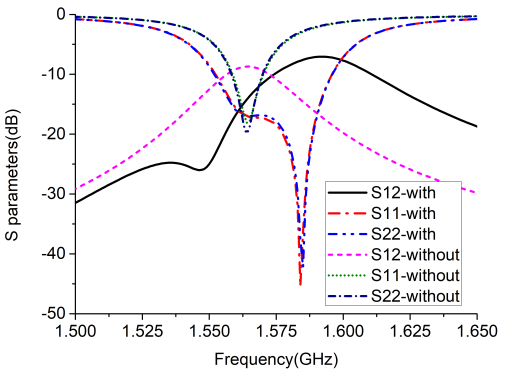

FIGURE 7. The antennas S-parameter comparison without and with the designed FDGS.

is better. Due to the antennas symmetric structures, the left placed CP transmitter antenna has the same parameter study conclusions when tuning the FDGS width and length.

III. OPTIMIZED SIMULATED RESULT COMPARISON

For better illustrate the achieved benefits of the proposed CP antennas, the antennas S-parameters and the antennas radiation patterns comparisons with and without the FDGS are shown in Fig. 7 and Fig. 8, respectively.

Fig. 7 indicates the optimized antennas S-parameters comparisons without and with the FDGS. Before etching the

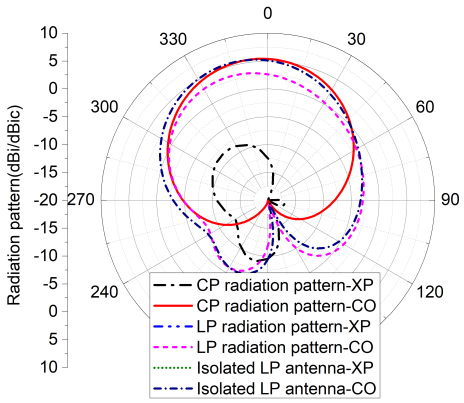

(a) *phi*=0deg plane

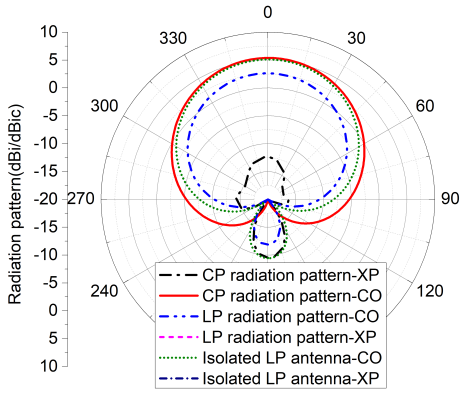

(b) *phi*=90deg plane

FIGURE 8. Radiation pattern comparisons of the right placed isolated LP antenna, as well as antennas without and with the proposed FDGS.

FDGS from the ground plane, the antenna works in the LP mode. When the antennas resonates in the GPS-L1 band, the 10-dB impedance bandwidths of the antennas with and without the FDGS are approximately 45 MHz and 10 MHz, respectively. Comparing to the LP antennas without the FDGS, the CP antennas with the FDGS have 35 MHz wider 10-dB impedance bandwidth. Which indicates the antenna impedance bandwidth broaden by this method. The presences of these two resonant modes contribute to expand the antenna 10-dB impedance bandwidth. This also results to the double minimum in the matching frequency behavior.

Fig. 8 (a) and (b) shows the radiation patterns of the isolated LP antenna, as well as the antennas without and with the FDGS in different planes. All those optimized results are calculated by the Ansoft HFSS, when only exciting the right placed antenna and 50 Ω load the other one. On the phi = 0 deg plane, the proposed CP antenna with the FDGS has more symmetric radiation pattern. In the phi = 90 deg plane, all three type antennas have symmetric radiation patterns in the upper-sphere space. The right placed isolated LP antenna, as well as the antennas without and with the FDGS have the forward realized gains 5.11 dBi, 2.56 dBi and 5.38 dBic, respectively. The isolated LP antenna and antenna with the FDGS have the more coincident radiation patterns on

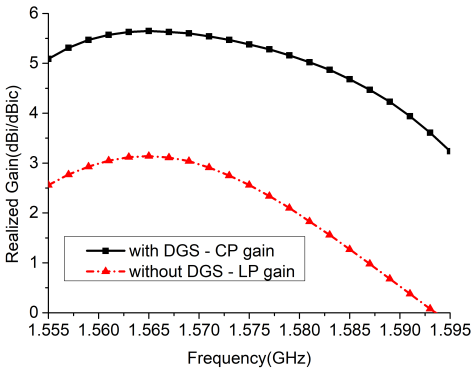

FIGURE 9. The forward realized gains against frequency of the antennas without and with the proposed FDGS.

both planes. Which indicates the FDGS application restores the antenna radiation patterns to the isolated antenna radiation patterns. Because of that, the antenna forward efficiency is increased from 66.8% to 81%, respectively. When only exciting the left placed antenna and 50 Ω load the other one, the same conclusion can be obtained because of the symmetric structure.

The forward realized gains values against frequency of the antennas without and with the proposed FDGS are plotted in Fig. 9. It clearly shows that the antenna with the FDGS has the increased realized gain within the GPS-L1 band. The antenna without the FDGS has the LP realized gain ranging from 2.34 dBi to 2.75 dBi within the GPS-L1 band. The antenna with the FDGS has the CP realized gain within the GPS-L1 band ranging from 5.28 dBic to 5.47 dBic. The antenna with the FDGS has a better efficiency performance within the GPS-L1 band. The proposed antennas forward efficiency are increased from 66.8% to 81%, when comparing to the antennas without the FDGS. The increased antenna realized gains and efficiencies are achieved due to the cradiation pattern restoration.

Comparing to the antenna without the FDGS, there are some benefits achieved by using the proposed FDGS for the CP antenna design: (1) The antenna CP operation is realized by etching the FDGS in the ground plane. (2) The designed CP antenna with the FDGS has more symmetric radiation patterns. Moreover, the radiation patterns of the designed CP antennas restore to that of the isolated antennas. (3) Due to the radiation pattern restoration, the designed antenna has improved forward realized gain and forward efficiency within the working band. When comparing to the corner-cut CP antennas, the designed CP antennas in this paper also have more symmetric radiation pattern, the increased forward realized gain and efficiency.

IV. SIMULATED AND MEASURED RESULTS COMPARISONS

Fig. 10 shows the fabricated CP antennas with the FDGS for the polarization diversity applications based on the optimized parameters. Both the patches connects to the SMA connectors

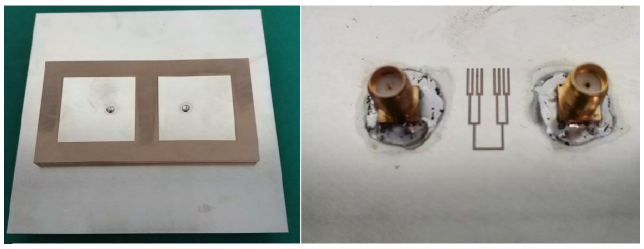

FIGURE 10. The fabricated CP antennas with the designed FDGS.

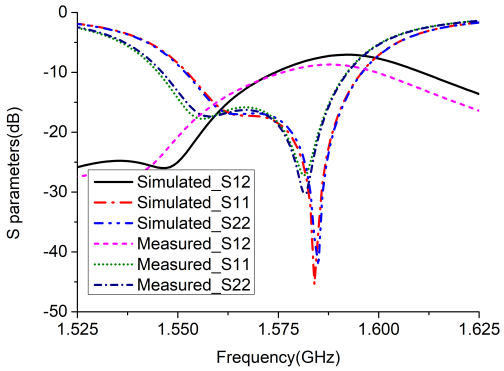

FIGURE 11. The measured and simulated S-parameter comparisons of the proposed CP antennas achieved by the FDGS.

and are printed on the same substrate. The CP antennas have the resonant frequency 1.575 GHz.

Fig. 11 gives the measured and simulated S-parameters of the proposed CP antennas with the FDGS. In general, the simulations agree well with the measurements. Both the simulated and measured results show that the designed antennas have 10-dB impedance bandwidth 45MHz, when the antennas have the center frequency 1.575GHz. Note that the measured S11 shifts to the lower frequency region, this may be caused by the substrate dielectric constant mismatch and the machine error.

Fig. 12 shows the measured and simulated antenna radiation patterns in the different planes, when only exciting the right placed CP antenna. The designed CP antenna is placed on a rotating platform in the anechoic chambers for the measurement, when the right positioned port is connected with the measured systems and the other port is connected with the 50Ω load. In both planes, the measured results coincide with the simulated ones. The results show that the designed antennas have the high-performance of the boresight radiation patterns. The proposed CP antennas have the 3-dB beamwidth approximately 90 deg and the forward CP realized gain 5.84 dBic.

Fig. 13 plots the measured and simulated antenna CP gains against the frequencies within the band of interest. The designed antenna has the simulated and measured forward CP realized gains 5.38 dBic and 5.84 dBic, respectively. Which indicates the good agreements between the simulations and measurements. The forward CP realized gains are relatively stable within the GPS-L1 bands. Fig. 13 also plots the

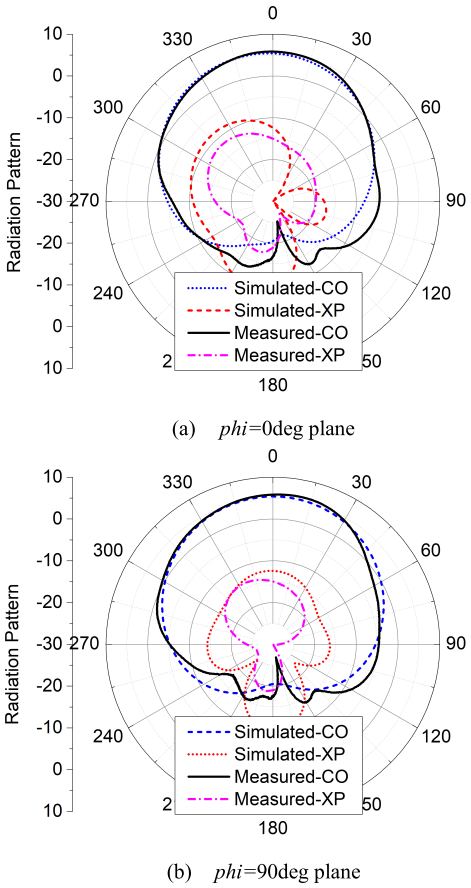

FIGURE 12. The measured and simulated radiation pattern comparisons of the right placed CP antenna with the FDGS in the different planes.

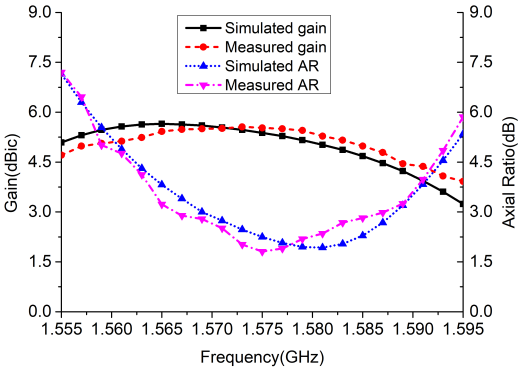

FIGURE 13. The measured and simulated antenna forward CP realized gains and forward ARs against frequencies.

simulated and measured forward ARs values against the frequency. It exhibits that the simulated and measured forward ARs values are 2.25 dB and 1.81 dB, respectively. Both the simulations and measurements results show that the designed antenna has the 3-dB AR bandwidth approximately 30 MHz.

V. CONCLUSION

The circular polarization diversity antennas with the restored radiation patterns are proposed in this paper. By etching

the designed FDGS away from the ground plane, the second orthogonal resonant mode for achieving the antenna CP operation is generated. This method of etching the FDGS also achieves the radiation patterns restoration, which helps to increase the antenna forward CP realized gains and the antenna forward efficiencies. The designed CP antennas have the 10-dB impedance bandwidth 45 MHz and the 3-dB AR bandwidth 30 MHz. Comparing to the antennas without the FDGS, the designed antennas have the increased antenna forward realized gain from 2.56 dBi to 5.38 dBic and the increased antenna forward efficiency from 66.8% to 81%, respectively.

REFERENCES

[1] M. Koohestani, A. Hussain, A. A. Moreira, and A. K. Skrivervik, "Diversity gain influenced by polarization and spatial diversity techniques in ultrawideband," *IEEE Access*, vol. 3, pp. 281–286, 2015.
[2] J. Malik, A. Patnaik, and M. Kartikeyan, "Novel printed MIMO antenna with pattern and polarization diversity," *IEEE Antennas Wireless Propag. Lett.*, vol. 14, pp. 739–742, 2015.
[3] S. W. Lee and Y. J. Sung, "Reconfigurable rhombus-shaped patch antenna with Y-shaped feed for polarization diversity," *IEEE Antennas Wireless Propag. Lett.*, vol. 14, pp. 163–166, 2015.
[4] Y. J. Sung, "Reconfigurable patch antenna for polarization diversity," *IEEE Trans. Antennas Propag.*, vol. 56, no. 9, pp. 3053–3054, Sep. 2008.
[5] K. Wei, J. Y. Li, L. Wang, R. Xu, and Z. J. Xing, "A new technique to design circularly polarized microstrip antenna by fractal defected ground structure," *IEEE Trans. Antennas Propag.*, vol. 65, no. 7, pp. 3721–3725, Jul. 2017.
[6] B. P. Chacko, G. Augustin, and T. A. Denidni, "Electronically reconfigurable uniplanar antenna with polarization diversity for cognitive radio applications," *IEEE Antennas Wireless Propag. Lett.*, vol. 14, pp. 213–216, 2015.
[7] S. Daoyi, J. J. Qian, H. Yang, and D. Fu, "A novel broadband polarization diversity antenna using a cross-pair of folded dipoles," *IEEE Antennas Wireless Propag. Lett.*, vol. 4, pp. 433–435, 2005.
[8] L. F. Zou and C. Fumeaux, "A cross-shaped dielectric resonator antenna for multifunction and polarization diversity applications," *IEEE Antennas Wireless Propag. Lett.*, vol. 10, pp. 742–745, 2011.
[9] J.-S. Row and Y.-H. Wei, "Wideband reconfigurable crossed-dipole antenna with quad-polarization diversity," *IEEE Trans. Antennas Propag.*, vol. 66, no. 4, pp. 2090–2094, Apr. 2018.
[10] H. H. Sun, H. Zhu, C. Ding, and Y. J. Guo, "Wideband planarized dual-linearly-polarized dipole antenna and its integration for dual-circularly-polarized radiation," *IEEE Antennas Wireless Propag. Lett.*, vol. 17, no. 12, pp. 2289–2293, Dec. 2018.
[11] C. Y. D. Sim, "Conical beam array antenna with polarization diversity," *IEEE Trans. Antennas Propag.*, vol. 60, no. 10, pp. 4568–4572, Oct. 2012.
[12] I. T. McMichael, "A mechanically reconfigurable patch antenna with polarization diversity," *IEEE Antennas Wireless Propag. Lett.*, vol. 17, no. 7, pp. 1186–1189, Jul. 2018.
[13] J. Liu, K. P. Esselle, S. G. Hay, Z. Sun, and S. Zhong, "A compact super-wideband antenna pair with polarization diversity," *IEEE Antennas Wireless Propag. Lett.*, vol. 12, pp. 1472–1475, 2013.
[14] H. Huang, Y. Liu, S. Zhang, and S. Gong, "Uniplanar differentially driven ultrawideband polarization diversity antenna with band-notched characteristics," *IEEE Antennas Wireless Propag. Lett.*, vol. 14, pp. 563–566, 2015.
[15] H. Huang, Y. Liu, S. Zhang, and S. Gong, "Uniplanar ultrawideband polarization diversity antenna with dual band-notched characteristics," *IEEE Antennas Wireless Propag. Lett.*, vol. 13, pp. 1745–1748, 2014.
[16] M. Koohestani, A. A. Moreira, and A. K. Skrivervik, "A novel compact CPW-fed polarization diversity ultrawideband antenna," *IEEE Antennas Wireless Propag. Lett.*, vol. 13, pp. 563–566, 2014.
[17] K. Wei and B.-C. Zhu, "The novel w parasitic strip for the circularly polarized microstrip antennas design and the mutual coupling reduction between them," *IEEE Trans. Antennas Propag.*, vol. 67, no. 2, pp. 804–813, Feb. 2019.

KUN WEI received the M.Sc. and Ph.D. degrees in electronic engineering from Northwestern Polytechnical University, in 2014 and 2017, respectively.

He currently holds postdoctoral position at the School of Electronics Engineering and Computer Science, Peking University. He authored more than 30 journal and conference papers in the last five years. His recent research interests include mutual coupling reduction, satellite communication antenna, circularly polarized antenna, metamaterial, and defected ground structure.

BOCHENG ZHU received the Ph.D. degree in electromagnetic field and microwave technology from the Beijing Institute of Technology, Beijing, China, in 1996. He is currently a Professor with the School of Electronics Engineering and Computer Science, Peking University, Beijing. He is a Senior Member of the Chinese Institute of Electronics. His research interests include wireless communication, satellite navigation, and microwave technology. He is a Senior Reviewer of the National High Technology Research and Development Program (863 Program) and the National Science and Technology Major Project of China.

MINGLIANG TAO received the B.Eng. degree in intelligent science and technology from Xidian University, in 2011, and the Ph.D. degree in signal processing from the National Laboratory of Radar Signal Processing, Xidian University, in 2016.

In 2016, he joined Northwestern Polytechnical University (NPU), as an Associate Professor. He authored more than 30 journal and conference papers in the last five years. His research interests include synthetic aperture radar imaging and data interpretation. He was a recipient of the Young Scientist Award from the International Union of Radio Science (URSI), the Postdoctoral Innovation Talent Support Program in China, and the Excellent Doctoral Dissertation Award from the China Education Society of Electronics, in 2017.